Spring phytoplankton bloom phenology during recent climate warming on the Bering Sea Shelf

Jens M. Nielsen[a,b,], Michael F. Sigler[c,+], Lisa B. Eisner[c], Jordan T. Watson[c,d], Lauren A. Rogers[b], Shaun W. Bell[e], Noel Pelland[a,b], Calvin W. Mordy[a,e], Wei Cheng[a,e], Kirill Kivva[f], Sage Osborne[a,e], Phyllis Stabeno[e]*

[a]*Cooperative Institute for Climate, Ocean, and Ecosystem Studies, University of Washington, Seattle, WA, United States*

[b]*National Oceanic and Atmospheric Administration, National Marine Fisheries Service, Alaska Fisheries Science Center, 7600 Sand Point Way NE, Seattle, WA 98115, USA*

[c]*National Oceanic and Atmospheric Administration, National Marine Fisheries Service, Alaska Fisheries Science Center, Auke Bay Laboratories, 17109 Point Lena Loop Rd, Juneau, AK 99801, USA*

[d]*Present Address: Pacific Islands Ocean Observing System, University of Hawai'i Manoa, 1680 East West Rd. POST 815, Honolulu, HI 96822, USA*

[e]*Pacific Marine Environmental Laboratory, NOAA, Seattle, WA, USA*

[f]*Russian Federal Research Institute of Fisheries and Oceanography, 19 Okruzhnoy proezd, Moscow, 105187, Russia*

[+]*(retired) Alaska Fisheries Science Center, National Marine Fisheries Service, Alaska Fisheries Science Center, Auke Bay Laboratories, 17109 Point Lena Loop Rd, Juneau, AK 99801, USA*

*Corresponding author email: jens.nielsen@noaa.gov

KEYWORDS: phytoplankton phenology, phytoplankton blooms, Bering Sea, ocean color, chlorophyll-a

ABSTRACT

High-latitude ecosystems commonly experience large phytoplankton blooms in spring, which provide basal resources for a range of grazers including zooplankton, benthic consumers and fishes. Variation of the timing and intensity of the spring phytoplankton bloom influences the degree of spatial and temporal overlap with consuming organisms. In the Bering Sea, blooms occur in association with ice retreat or as pelagic open-water blooms. In the last few years, the Bering Sea shelf experienced unprecedented and widespread warming. Understanding how those climatic changes subsequently influenced phytoplankton bloom dynamics is critical for evaluating Bering Sea food web responses. We estimate spring bloom timing and type (ice-associated, open-water) across the Bering Sea shelf using a combination of data from the long-running oceanographic moorings on the eastern shelf (M2, M4, M5, M8) and satellite ocean color data from 1998 to 2022. We assess 1) if the Bering Sea shelf experienced noticeable changes in spring bloom timing or type in the last two decades, 2) whether bloom phenology was accentuated by the recent warm period (2018-2019), and 3) what influences do winds have on spring bloom timing and where are these variables influential? Our spatial analyses reinforce the conclusion that ice retreat is the dominant forcing factor of bloom timing for the Bering Sea shelf with some influence of wind for open-water blooms. Overall, bloom timing has not shifted seasonally with climate warming in the last two decades for most of the Bering Sea shelf, except for nearshore areas and mainly in the Northern Bering Sea. In warm years when ice retreats

early prior to the last week of March, blooms form in open waters and bloom timing on the middle and outer shelf is delayed when wind mixing is prevalent in ice-free springs. In recent years, open-water blooms were more widespread than previously experienced, and even occurred in the Northern Bering Sea during 2018-2019. A progression to more open water blooms in a future warmer climate will influence the availability of basal resources for pelagic and benthic consumers.

1. Introduction

Marine ecosystems in higher latitudes have high seasonality and commonly experience intense phytoplankton blooms in spring (Ji et al., 2010; Ji et al., 2013; Song et al., 2021). Spring phytoplankton blooms provide indispensable basal resources for a range of grazers including zooplankton (Kimmel et al., 2018; Sigler et al., 2016; Staudinger et al., 2019), benthic consumers (Copeman et al., 2021) and fishes (Friedland et al., 2019; Hunt et al., 2011). The timing and intensity of phytoplankton blooms vary due to changing environmental factors (Ji et al., 2010), such as ice retreat, nutrients, light, water temperature, stratification and wind mixing (Chiswell et al., 2015; Stabeno et al., 2012a; Stabeno et al., 2012b). Shifts in bloom intensity and phenology influence the degree of spatial and temporal overlap with consuming organisms (Cushing, 1990; Ferreira et al., 2020; Hunt et al., 2011; Kharouba et al., 2018), which in turn have propagating effects on marine food web structure and function (Chmura et al., 2019; Staudinger et al., 2019).

Arctic and subarctic ecosystems, including the Bering Sea, are in transition due to rising temperatures and associated sea-ice loss (Ballinger and Overland, 2022; Duffy-Anderson et al., 2019; Mueter et al., 2021). The eastern Bering Sea shelf is a highly productive ecosystem

(Springer et al., 1996) that extends about 500 km from the Alaska coast to the continental shelf break. The shelf gradually slopes, increasing in depth from east to west with a depth of ~180 m near the shelf break. The Bering Sea shelf is often divided into several domains encompassing the inner (0-50 m bottom depth), middle (50-100 m) and outer shelf (100 - 180 m) and between north (> 60 °N) and south (< 60 °N). This division of domains, while somewhat arbitrary, is due to differences in oceanographic characteristics (Baker et al., 2020), such as tide strength, currents, and nutrients (Stabeno et al., 2012a). The timing of sea-ice retreat is a primary driver of spring bloom formation in the northern Bering Sea (Kivva et al., 2020; Stabeno and Bell, 2019) as well as in other Arctic and sub-arctic ecosystems (Song et al., 2021; Waga et al., 2021). Historically, in the southern Bering Sea, ice-associated blooms occur in cold years with extensive ice coverage, while in warm years when ice retreats earlier than mid- to late-March, open-water blooms form several weeks after ice retreat (Brown and Arrigo, 2013; Niebauer et al., 1995; Sigler et al., 2014). Physically, the stratification associated with an ice edge bloom forms when ice melting freshens the sea surface (Niebauer et al., 1995), while open-water blooms occur at the onset of temperature induced water column stratification, influenced by a combination of increases in solar radiation and relaxation of winds (Ladd and Stabeno, 2012; Sambrotto et al., 1986). In the northern Bering and Chukchi seas, ice-associated blooms form under the ice or as marginal ice edge blooms that peak shortly after ice retreat (Arrigo et al., 2014; Waga et al., 2021). However, unusual warming in 2018 and 2019 due to large-scale climatological shifts in the region (Ballinger and Overland, 2022; Basyuk and Zuenko, 2020) resulted in early ice-retreat (Baker et al., 2020) and thus areas of open-water blooms occurring more than three weeks after sea-ice break up in the northern Bering Sea (Kivva et al., 2020). Such changing bloom dynamics, both in terms of timing, and whether the bloom forms in

association with the ice or in open water, have large-scale effects on nutritional quality and distribution of food resources available for benthic and pelagic organisms (Hunt et al., 2011; Koch et al., 2020).

To better understand how the Bering Sea shelf will respond to projected future climate scenarios of warmer waters and reduced ice extent, we assess spring phytoplankton bloom dynamics across the entire Bering Sea shelf. First, we combine information from the long running oceanographic moorings in the eastern Bering Sea (M2, M4, M5, M8, Fig. 1) with satellite ocean color data from 1998 to 2022, and compare spring bloom peak timing estimates. Next, we address the following three questions:

1) Has the Bering Sea shelf experienced noticeable changes in phytoplankton spring bloom timing and bloom type (ice associated or open water) in the last two decades, and are there distinct differences north to south and east to west?

2) How did the recent warm period (2018-2019) influence bloom dynamics?

3) Beyond ice retreat timing, how do winds and ocean sea surface temperatures influence spring bloom timing and where are these variables most influential across the Bering Sea shelf ecosystem?

If shifts in the phenology or primary driving factors of the spring bloom are occurring in the Bering Sea due to warming, it could indicate widespread ecosystem changes that may culminate in larger-scale trophic reorganization.

2. Methods

87 *2.1. Data*

88 Bloom dynamics were assessed from 1998 to 2022 for the Bering Sea shelf (here defined as the
89 eastern Bering Sea and Anadyr Bay areas with bottom depth shallower than 180 m, from north of
90 the Aleutian Islands to the Bering Strait). We compiled 8-day satellite chlorophyll-a (Chl-*a*, ug l^{-1})
91 at a 4 km-resolution from The Hermes GlobColour website (http://hermes.acri.fr/, Maritorena
92 et al., 2010). This is a standardized merged Chl-*a* product, combining remote sensing data from
93 SeaWiFS, MERIS, MODIS, VIIRS and OLCI. Chl-*a* data covering the Bering Sea shelf region
94 (20-180 m, Fig. 1) were binned and averaged into ~0.5° (56 km) latitude × 1° (47 - 65 km)
95 longitude grid cells. The size of the grid cells was chosen to include enough satellite pixels to
96 assess spatial bloom variation across the shelf. Any individual satellite pixels that had more than
97 10% ice cover were excluded from the bloom timing analysis as this can yield highly uncertain
98 Chl-*a* values (Brown & Arrigo 2013). Because data were binned, there were instances where
99 Chl-*a* data were present in a bin, even when average ice concentrations for a bin were above 10
100 %. Locations shallower than 20 m bottom depth and near river plumes from the Yukon,
101 Kuskowim, and Anadyr rivers also were excluded, following recommendations in Brown et al.
102 (2011). Sea surface temperature (SST, C°, 5 km-resolution,
103 https://coastwatch.pfeg.noaa.gov/erddap/griddap/NOAA_DHW.html, Skirving et al. (2020)), and
104 ice coverage (0-100%, 5 km-resolution,
105 https://coastwatch.pfeg.noaa.gov/erddap/griddap/NOAA_DHW.html, Skirving et al. (2020)) data
106 were compiled from 1 Jan to 31 July for the years 1998 to 2022 and spatially binned into the
107 same grid cells as the Chl-*a* satellite data. We used wind speed data (m s^{-1}) at 6 h resolution from
108 NCEP/NCAR Reanalysis 1 (https://psl.noaa.gov/data/gridded/data.ncep.reanalysis.surface.html,
109 Kalnay et al. (1996)) at ~ 2° (94 -131 km longitude × 222 km latitude) spatial resolution that

were then assigned to the nearest satellite Chl-*a* grid cells. Wind speeds from the Reanalysis 1 compare well to independent buoy wind speed measurements including data at M2 (Ladd and Bond, 2002), and using a higher than daily resolution works well for capturing sporadic wind events. While satellite data provide unique spatio-temporal coverage, these products often have missing data due to clouds and ice cover, thus to validate the bloom timing estimates we compared the satellite bloom timing estimates to mooring bloom timing estimates (Chl-*a* derived from factory-calibrated fluorescence sensors) at four locations (Fig. 1). We used data from the long-term moorings M2 (56.87°N, 164.05°W), M4 (57.90°N, 168.87°W), M5 (59.92°N, 171.73°W) and M8 (62.19°N, 174.69°W) for the time-period (1998-2022), though gaps were present for certain mooring locations and years.

2.2. Spring bloom timing, ice retreat and wind intensity estimates

The timing of the peak of the spring bloom was estimated for each year and spatial location (satellite grid cell or mooring location). For a given satellite grid cell, Chl-*a* was natural log+1 transformed, hereafter L(Chl-*a*), and linearly interpolated in time. The spring bloom peak was defined as the highest peak of the 8-day curve between day of year 60 (~1 March) and 180 (~1 July). Spring peak bloom timing was only determined for a grid cell in a given year if the peak reached L(Chl-*a*) values > 0.69, equivalent to a Chl-*a* value > 1 $\mu g\ l^{-1}$, a threshold value that works well for coastal and shelf regions (Dai et al., 2023). In addition, grid cells that had temporal gaps in satellite data larger than three 8-day composites were excluded from the analysis. Mooring spring bloom peak timing was similarly estimated but using a 8-day running L(Chl-*a*) mean of daily averaged data. Moored fluorescence sensors were deployed during summer (early May to late September) and winter (late September to early May) at a water depth

of ~10 m. Exceptions were winter data (when then the water column is usually well mixed) from the M8 mooring where sensors were deployed at 21-22 m to avoid ice keels. During the spring, the bloom is present from surface and below the depth of these moorings, and thus the use of sensors at these depths are reliable indicators of the bloom peak (Sigler et al., 2014).

A categorical variable was used to denote "bloom type" which differentiated between open-water blooms (ice retreat occurred equal to or more than 21 days prior to bloom peak) and ice-associated blooms (ice retreat occurred less than 21 days prior to bloom peak) for each year and location. The threshold value for bloom type of 21 days was used because ice edge blooms commonly form within 21 days of ice retreat (Perrette et al., 2011; Sigler et al., 2014). Ice-associated blooms encompass bloom peaks occurring during ice retreat or within the few first weeks after ice retreat. Timing of sea-ice retreat was determined as the date when ice coverage remained below 15% based on the 8-day running mean of the daily sea-ice fraction data. We also calculated the average percent ice cover from 1 January to the time of ice retreat for each grid cell as a measure of ice coverage consistency.

A wind intensity metric was calculated as a relative metric to assess the influence of spring storms that were expected to keep the water column from stratifying and thus delay the bloom formation. The wind metric was calculated as the cumulative sum score of all wind speed events during April and May at above 10 m s^{-1} occurring for at least 24 hours. Thus, the wind metric scored all wind speeds < 10 m s^{-1} as 0, winds speeds >15 m s^{-1} was counted as an upper threshold value of 15 m s^{-1}, and all values between 10-15 m s^{-1} were scored as that specific wind speed in m s^{-1}. Note that the wind metric is a relative cumulative metric over a 2-month period. In the last two decades the Bering Sea have experienced large scale multiyear environmental changes, consisting of an early warm (2001-2005), a cold (2006-2013) and a recent warm period

(2014-2021, Stabeno and Bell 2019). In addition, to assessing inter-annual variability of temperature variation at each spatial location, we determined the cumulative April-May SST anomaly for each grid cell, relative to that grid cells cumulative long-term April-May SST average value.

2.3. Model analyses of factors affecting bloom type and timing

2.3.1 Bloom type decision tree analysis

We assessed which factors influence the formation of ice associated or open-water blooms, using decision tree analysis to fit a binary classification model on the bloom type categories (Breiman et al., 2017). Decisions tree models were fit separately for the Northern (> 60° N) and Southern Bering (< 60° N) sea, where,

Bloom type ~ ice retreat timing + wind metric + latitude + bottom depth + cumulative SST anomaly (1)

and bloom type constitutes the predictive target for binary classification and the factors ice retreat timing, cumulative wind metric, latitude, cumulative SST anomaly and bottom depth are used as classification features. Data for the decision tree analysis was randomly split 70/30 into two data sets, a training dataset and a test dataset, respectively. The values of the classification features in the training dataset were used to fit a decision tree following recursive partitioning scheme, i.e. classification of data by splitting it into subgroups (bloom type) based on a number of predictor variables, which terminates once the partitions derived from input data are no longer informative. After the model was fit on the training dataset, the out-of-sample performance was evaluated by computing the model sensitivity. This was done by applying the fitted model to the

178 test dataset and calculating the true positive rate (which is robust to disproportionate
179 representation of either category in the data) of bloom type categories from the corresponding
180 confusion matrix (Breiman et al., 2017), which summarizes the number of correct and incorrect
181 predictions of bloom type made by the decision tree analysis.

182

183 *2.3.2 Generalized additive models (GAMs)*

184 Bloom timing was analyzed with GAMs to assess how spring bloom peak timing (T) is related to
185 ice retreat timing (ice), type of bloom (bloomtype), cumulative April-May wind speed intensity
186 (wind), and April-May cumulative SST anomaly (sst). We explored four spatial GAMs with
187 different levels of complexity. The first model (Model A), our most basic model explored how
188 ice retreat timing influence bloom timing, as ice is a known main driver of bloom timing (Sigler
189 et al., 2014). Next (model B), we explored if and how bloom timing is influenced by the factors,
190 ice retreat, cumulative SST anomaly and wind speed intensity. The third and fourth GAM
191 models, termed spatially-varying coefficient models, explored specifically how the influence of
192 ice retreat (model C) and winds (model D) influence bloom timing across space. Note that for
193 model D we focused on bloom timing when open water blooms occurred. All models were
194 additional fitted with categorical (e.g. *bloom type*) and random factors (e.g. *year*) when deemed
195 relevant. Each model included a two-dimensional spatial smooth function (g) of latitude (ϕ) and
196 longitude (λ), modeled as a tensor product. The effects of single covariates were modeled as thin
197 plate regression splines (s), and errors (e) were normally distributed.

198 our first model (model A) considered bloom peak timing as a function of ice retreat
199 timing and location, with *year* as categorical random effect:

$$T_{y,(\phi,\lambda)} = s_1\left(ice_{y,(\phi,\lambda)}\right) + g_1(\phi,\lambda) + year_y + e_{y,(\phi,\lambda)} \,. \quad (2)$$

Next, we constructed the full model (model B) to explore if additional parameters beyond ice retreat influenced bloom timing. Because the influence of ice-retreat timing, the number of storm events and temperature likely varies depending on whether a bloom is ice-associated or occurs in open water, the full model allowed the effects of those variables to differ by bloom type. In this formulation, I is an indicator variable distinguishing open-water versus ice-associated blooms, and bloom type is included in the model as a factor:

$$T_{y,(\phi,\lambda)} = I_1 s_1\left(ice_{y,(\phi,\lambda)}\right) + I_2 s_2\left(ice_{y,(\phi,\lambda)}\right) + I_1 s_3\left(wind_{y,(\phi,\lambda)}\right) + I_2 s_4\left(wind_{y,(\phi,\lambda)}\right) +$$

$$I_1 s_5\left(sst_{y,(\phi,\lambda)}\right) + I_2 s_6\left(sst_{y,(\phi,\lambda)}\right) + bloomtype_{y,(\phi,\lambda)} + g_1(\phi,\lambda) + year_y + e_{y,(\phi,\lambda)} \,. \quad (3)$$

Model selection using Akaike Information Criterion with correction for sample size (AICc, Burnham and Anderson (2002)) revealed the full model as the most parsimonious model.

Using the parsimonious model B structure, we then explored where ice retreat (model C) and cumulative wind speed (model D) were most influential across space. This was investigated using spatially-varying coefficient GAMs, where the effects of ice retreat timing or cumulative wind speed were modeled as linear effects with the slope allowed to vary across space.

The first spatially-varying coefficient GAM, model C, includes a spatially-varying effect of ice retreat on bloom timing. Bloom type is included in the model as a factor:

$$T_{y,(\phi,\lambda)} = g_1(\phi,\lambda) + g_2(\phi,\lambda) * ice_{y,(\phi,\lambda)} + s_1\left(wind_{y,(\phi,\lambda)}\right) + s_2\left(sst_{y,(\phi,\lambda)}\right) +$$

$$bloomtype_{y,(\phi,\lambda)} + year_y + e_{y,(\phi,\lambda)} \,. \quad (4)$$

The second spatially-varying coefficient GAM, model D, includes a spatially-varying effect of cumulative wind speed on bloom timing and was modeled using only open-water bloom data (ice retreat occurred more than 21 days prior to bloom peak):

$$T_{y,(\phi,\lambda)} = g_1(\phi,\lambda) + g_2(\phi,\lambda) * wind_{y,(\phi,\lambda)} + s_1\left(sst_{y,(\phi,\lambda)}\right) + s_2\left(ice_{y,(\phi,\lambda)}\right) + year_y + e_{y,(\phi,\lambda)} \quad (5)$$

All data analyses were performed with the statistical software R 3.6 (R Core Team, 2018) and associated packages, using *mgcv* (Wood and Wood, 2015) for the GAM analysis, *dplyr* (Wickham et al., 2019), *ggplot2* (Wickham and Chang, 2009) for statistical analysis and plotting, and *rpart* (Therneau et al., 2015) for the decision tree analysis.

3. **Results**

3.1. Satellite-mooring comparison

Spring bloom timing from satellite Chl-*a* agreed well with estimates based on the surface (10-22 m) mooring Chl-*a* data from the M2, M4, M5 and M8 moorings ($r = 0.75$, $p < 0.01$, Fig. 2A-E). Although the bloom timing estimates were highly correlated, there were several years where smaller secondary spring peaks were evident in the mooring data, events that were not always captured by the satellite Chl-*a* data. Such smaller secondary blooms occurred in, for example, 2007, 2011 and 2016 at M2 (Fig. S1). For both satellite- and mooring-based estimates (Fig. 2A-B), at the southern mooring locations (M2, M4), open-water blooms generally occurred during 2001-2005 (except for M4 in 2003) and from 2014 onwards (except for 2017). Ice-associated blooms frequently occurred during 2006-2013, except in 2006, 2009, and 2011 at M2 and in 2007 at M4 (Fig. 2 A-B). At the northern mooring locations (M5, M8), ice-associated blooms occurred

241 during most years (1998-2017), with open-water blooms occurring since 2018 for M5 and in
242 2018-2019 for M8 (Fig. 2C-D).

243

244 *3.2. Spring bloom timing, ice retreat and cumulative wind intensity*

245 Satellite estimates for the Bering Sea shelf showed that the bloom peak on average occurred
246 earliest in the southeast and then progressed towards the northwest (Fig. 3A). On the southern
247 shelf the estimated bloom peak occurred first on the inner shelf, then the middle shelf, and then
248 progressing to the outer shelf (Fig. 3A). Bloom timing varied among years and across space (Fig.
249 S2), but peak timing generally remained between mid-April to mid-June (a 60-day window) with
250 no trend across the time-period. In addition, there was some evidence that warmer temperatures
251 affected bloom timing differently offshore versus inshore (Fig. 3B). In inshore areas and in the
252 Northern Bering Sea, warmer temperatures were associated with earlier blooms, whereas in a
253 few offshore areas warmer temperatures linked to later blooms. Statistically significant
254 correlations were present in about one third of the total area most of which was confined to the
255 nearshore and primarily in the northern Bering Sea (Fig. 3B).

256 Since the start of our satellite time-series (1998 to 2022) the Bering Sea have experienced
257 several multi-year cold (2006-2012) and warm periods (2001-2005, 2014-2021, Fig 4A). Periods
258 with warmer ocean temperatures experienced earlier ice retreat (Fig 4B) and higher frequencies
259 of open water blooms (Fig 4C). The spring bloom generally occurred in two forms: an open-
260 water bloom, or an ice-associated bloom regulated by the timing of ice retreat (Fig. 4, Fig. 5). In
261 rare cases (< 3 %) the bloom was estimated to occur prior to the estimated ice retreat timing
262 (diamonds, Fig. 5). In those instances, ice coverage was not consistent throughout spring, as ice

263 would retreat and advance across a location, providing periods of open water where Chl-*a*
264 accumulation could occur (Fig. S3).

265 Satellite bloom timing was closely coupled to ice retreat during cold years (Fig. 5B,
266 example years 2010-2012); also seen in the mooring analysis (Fig. 2F). In contrast, open-water
267 blooms uncoupled from ice retreat occurred more frequently in warm years with early ice retreat
268 (Fig. 5A, 2003-2005 example years). During the recent warm period (2018-2020) with early ice
269 retreat, large parts of the Bering Sea shelf bloom were uncoupled from ice retreat (Fig. 5C), and
270 covered a much larger area than the earlier warm years (2001-2005). During most years (1998-
271 2016, 2020-2021), the area of open-water blooms was always below 22% on the northern Bering
272 Sea shelf (> 60° N). However, the exceptional recent warming resulted in much larger portions
273 of the northern shelf being occupied by open-water blooms in 2017 (38%), 2018 (82%), and
274 2019 (46%). Ice fraction, a measure of the consistency of ice coverage, also differed between the
275 recent warm period (Fig. 5C) and the earlier warm period (Fig. 5A).

276 Decisions tree analyses of the satellite estimates for the Bering Sea shelf showed that
277 bloom type (either open water or ice associated) was primarily influenced by ice retreat timing.
278 For the southern Bering Sea open-water blooms consistently occurred when ice retreat was
279 before 30 March (56% of the data), whereas ice-associated blooms consistently occurred when
280 ice retreat was after April 23 (33% of total bloom types, Fig. 6A, decision tree classification
281 analysis, 89% classification accuracy). Between 30 March and 23 April, bloom type varied with
282 bottom depth, with ice-associated blooms occurring in the inner shelf (>55 m, 4 % of the time)
283 while open-water blooms occurred on the middle and outer shelf (7 %). In the northern Bering
284 Sea (latitude > 60 °N), ice associated blooms occurred if ice was present after 9 May (65 % of
285 the data, Fig. 6B, decision tree classification analysis, 87% classification accuracy). Between 16

April and 9 May, ice associated blooms occurred in the northern Bering Sea below latitude 65 °N (25 %), while open water blooms (2 %) formed between 65 – 65.6 °N (the Bering Strait region). Open water blooms occurred if ice retreat was prior to 16 April (8 %). Overall, open water blooms were rare in the northern Bering Sea (10 % of all the data).

Higher cumulative wind speeds during April-May, an indicator of stormier springs, significantly delayed bloom occurrence in the southern Bering Sea in both early and recent warm years (e.g., 2001-2005, 2018-2020, respectively, Fig. 7), whereas in cold years (e.g., 2010-2012) there was no delay due to the wind. In the northern Bering Sea, wind speeds were weakly explanatory in both cold and warm periods but with no clear trends (low r^2, Fig. S4).

3.3. Factors affecting bloom timing: GAM analyses

GAM analyses showed that bloom timing correlated with ice retreat timing and subsequently, the bloom is further influenced by additional factors, most notably cumulative winds for open-water blooms (Fig. 8). Model A, the GAM including only ice retreat and year as a random effect, explained 52 % of the deviance (Deviance explained = 52.0 %, n = 5335), supporting the conclusion that ice retreat is a primary regulator of bloom timing. The full GAM (Model B) showed that ice retreat, cumulative wind speeds, and cumulative SST anomalies, with bloom type and year as random effects, explained significant variation in bloom timing (Deviance explained = 60.4%, n = 5335, Fig. 8). Bloom timing was positively associated with ice retreat timing for both open-water and ice-associated blooms (Fig. 8A, 8D). Higher cumulative wind speeds significantly delayed the open-water bloom (Fig. 8B), but did not significantly influence the timing of ice associated blooms (Fig. 8E). The wind effect for open-water blooms was

minimal for cumulative spring wind speed values below ~ 500 m/s, indicating that bloom timing was not delayed when few spring storms occurred. Cumulative SST anomaly was a significant term in the most parsimonious model (Fig. 8C, 8F), but the effect was minor for both open-water and ice associated blooms.

Next, using the spatially-varying coefficient GAMs, we assessed the influence of ice retreat timing (Model C) and wind speed (Model D) across the shelf. Spatially, ice retreat timing (model C, Deviance explained = 58.8 %, n = 5335) was positively correlated with bloom timing in the northern Bering Sea (Fig. 9A). In the southern Bering Sea, ice retreat correlated positively with bloom timing on the inner shelf and the shallower part of the middle shelf, but not the outer shelf (Fig. 9A). Higher cumulative wind speeds (model D) delayed open-water bloom timing on the middle and outer shelf especially in the south (< 60°N) (Fig. 9B, Deviance explained = 46.6 %, n = 2116). In contrast, open-water bloom timing was earlier with higher cumulative wind speeds on the inner shelf in a smaller region around Nunivak Island, just south of the Bering Strait and in the Gulf of Anadyr.

4. Discussion

Our spatial analysis of spring bloom timing for the Bering Sea shelf shows that ice retreat is the dominant factor affecting bloom timing, matching conclusions from past studies (Brown and Arrigo, 2013; Sigler et al., 2014). The timing of ice retreat dictates bloom timing on the Bering Sea shelf, except when ice retreat occurs early, prior to the end of March, which commonly happens in warmer years in the south (< 60 °N) and so far, only rarely in the north (e.g., 2018 and 2019). During years with early ice retreat, our analyses show that stronger spring winds

delay the open-water bloom across the southern middle and outer shelf areas. The Bering Sea shelf experienced noticeable changes in phytoplankton spring bloom type between cold and warm periods (Fig. 4C), but there was no trend in spring bloom timing in the last two decades. In the recent warm years with very low sea-ice coverage (2018 and 2019), open-water blooms formed over much larger areas than previously observed, particularly in the northern Bering Sea (Stabeno and Bell, 2019; Stabeno et al., 2012b).

4.1. Bloom timing dynamics on the Bering Sea shelf

Assessing our first objective, if there has been noticeable bloom changes in the past decades, we find that blooms across the Bering Sea occur inter-annually within 60-day window (mid-April to mid-June), concurring with previous satellite (Brown and Arrigo, 2013) and observational studies from previous decades (Niebauer et al., 1995). However, for a given location the variation of bloom timing varied about 2-4 weeks. Commonly, bloom formation starts on the inner shelf, before occurring on the middle and then the outer shelves. The directional bloom progression across the shelf is most visible in the southern Bering Sea and concurs with previous observations on spatial differences in bloom timing (Coachman, 1986; Kivva and Kubryakov, 2021; Niebauer et al., 1995) though observations on inner shelf bloom dynamics are more scarce (Stabeno and Hunt, 2002).

In the northern Bering Sea (> 60° N) blooms have historically been associated with ice-retreat (Stabeno and Bell, 2019). Blooms associated with ice are commonly larger aggregates that form as thick under ice blooms (Arrigo et al., 2014; Stabeno et al., 2020), or are associated with the ice edge meltwater during retreat (Waga et al., 2021). Such bloom dynamics occur

predominantly in the Pacific, marginal and central Arctic oceans (Ji et al., 2013; Song et al., 2021). Recent observations show that earlier ice retreat in the Arctic Ocean results in earlier bloom timing (Kahru et al., 2011; Kahru et al., 2016; Song et al., 2021) as well as a shift from under ice to marginal ice blooms in the northern Bering Sea (Waga et al., 2021). Our analyses agree with these observations for the northern Bering Sea. Although an exception to that pattern occurred in the low ice years of 2018 and 2019 when open- water blooms were common in the northern Bering Sea.

For the southern Bering Sea, our results show that if ice retreat occurs after late March, the timing of ice retreat regulates the timing of ice-associated blooms. If ice retreat is early (prior to late-March) open-water blooms form with increasing solar radiation and relaxation of local winds, in agreement with previous studies (Brown and Arrigo, 2013; Hunt et al., 2011; Niebauer et al., 1995; Saitoh et al., 2002; Stabeno et al., 2012a). On average, open-water blooms occur slightly later than ice-edge blooms (Niebauer et al., 1995). The relaxation of the winds enhances water column stratification and the light levels over the surface mixed layer become non-limiting for phytoplankton growth and accumulation of biomass (Chiswell et al., 2015). While bloom timing is generally variable but constrained within a 2-month period there are a few exceptions to this pattern. For example, in areas near the M4 mooring in 2003, a warm year, an open-water bloom occurred exceptionally early at the beginning of April (day 94), as also noted previously in both satellite and mooring observations (Brown and Arrigo, 2013; Sigler et al., 2014).

Evaluating the second objective, we show that the frequency of open-water blooms across the Bering Sea increased during the recent warm period, and particularly in 2018-2019 (Fig. 4C). Open-water blooms were the dominant type in the southeastern Bering Sea during 2001-2005 as well as in the recent warm period (2014-present). Studies of the northern Bering

375 Sea published prior to the recent warm period suggested this region would remain seasonally ice
376 covered (Stabeno et al., 2012a; Stabeno et al., 2012b) and continue to be dominated by ice
377 associated blooms (Brown and Arrigo, 2013). However, in 2018-2019 sea ice was extremely
378 limited (Ballinger and Overland, 2022; Stabeno and Bell, 2019) and we observed open-water
379 blooms much more widespread across the northern Bering Sea, something not seen previously,
380 including the early warm years 2001-2005. Given future climate projections (Cheng et al., 2021)
381 a northward expansion of open-water blooms during warm years indicates that the northern
382 Bering Sea could eventually experience bloom dynamics more like the southern Bering Sea and
383 less like Arctic regions. That is, in future open-water blooms may occur in warm years in the
384 northern Bering Sea due to early ice retreat, while ice-associated blooms will continue to form in
385 colder years.

386 When open-water blooms occur, our analyses show that the intensity of the winds in
387 spring becomes a regulating factor on the middle and outer shelf, acting to delay the bloom as
388 winds intensify. The recent warm period and associated record low sea-ice extent (2018-2019)
389 appear to be the results of larger scale climatological shifts in the region (Ballinger and
390 Overland, 2022). Future projections indicate that surface winds may increase in subpolar and
391 polar regions (Mioduszewski et al., 2018), along with increased poleward ocean heat transport
392 and northward retreat of the ice edge (Alkama et al., 2020). While wind projections carry notable
393 uncertainties (Walsh et al., 2020), it appears that spring wind intensities will play an increasing
394 role in regulating bloom timing as open-water blooms become more prevalent throughout the
395 Bering Sea, particularly during climatological conditions comparable to those experienced after
396 2017 (Ballinger and Overland, 2022).

397

4.2. Challenges of estimating large scale bloom dynamics

Overall, bloom timing estimated from mooring and satellite ocean color data were in good agreement with each other. Nonetheless, while satellite data provide extensive spatial and temporal coverage, these estimates are limited to surface waters and clouds and ice-cover may impact the accuracy of the Chl-*a* estimates (Cole et al., 2012). Thus, our analysis does not cover phytoplankton processes occurring below the ice or in association with subsurface blooms which are prevalent in large areas of the eastern Bering Sea after the spring bloom period (Eisner et al., 2016; Stabeno et al., 2012a). While our analysis from mooring and nearby satellite estimates of Chl-*a* identified similarity in the timing of bloom peaks, it was also evident from the mooring data that smaller secondary peaks occur in some years. While smaller in overall magnitude compared to the main bloom peak, these blooms can still be important ecologically, particularly if such short upswings in phytoplankton accumulation occur at a time where resources for consumers, such as zooplankton, are otherwise limited. In addition, we focused on meso-scale bloom patterns (~50-100 km) and thus may have missed small-scale variation (patchiness) in bloom dynamics as well as finer-scale ice dynamics. Thinning ice thickness in areas still ice covered may also influence bloom dynamics, and ice cover is known to expand and retract throughout the winter and spring, which adds complexity to the ice retreat timing estimates as well as causes short-term pulses of released ice-associated algae (Syvertsen, 1991). Our approach did not consider changes to ice thickness and how that might influence under-ice bloom dynamics and bloom type and timing. Nonetheless, our analysis was still capable of depicting spring bloom phenology and associations to dominant physical processes across the Bering Sea shelf.

4.3. Implications for the Bering Sea ecosystem dynamics

The spring bloom is associated with most of the annual primary production and consequently, the amount of organic carbon leaving the euphotic zone (Hunt et al., 2011; Saitoh et al., 2002; Sigler et al., 2014). Our analysis shows that bloom timing on the Bering Sea shelf occurs within a 2-month period and that there has been no trend in bloom timing despite a wide range of climate conditions in the last 25 years, a pattern that is consistent with earlier data from the 1980s and 1990s (Niebauer et al., 1995). Yet, our analysis, showed that open-water blooms occurred more frequently in recent years and across a larger area of the Bering Sea shelf. While bloom timing remains without a long-term trend, consumer development times (e.g., copepod stage progression) and diapause dynamics are tightly coupled to ambient water temperatures (Coyle and Gibson, 2017; Pierson et al., 2013). If consumers experience phenological shifts, due to shorter development times and reduced diapause extent with rising temperatures while the bloom timing is largely unchanged, it can still change phenological synchrony between consumers and their resources (Kharouba et al., 2018), which will have subsequent effects on secondary production.

The prevalence of open-water blooms is likely to increase and result in an increasing proportion of phytoplankton adapted to pelagic conditions (Grebmeier et al., 2018). This will likely also cause a reduction of ice-associated algae of high nutritional quality that are ecologically important for lipid-rich crustacean zooplankton (e.g., *Calanus* sp. copepods (Baier and Napp, 2003)) and euphausiids (Hunt et al., 2016), which are major prey resources for fishes, seabirds, and marine mammals (Hunt et al., 2011; Sigler et al., 2016). The 2001-2005 warm period prompted several subsequent years of decline for cold-water species such as large lipid-rich copepods (Eisner et al., 2020). Moreover, juvenile pollock survival was reduced (Siddon et

al., 2013) and adult pollock abundance halved (Ianelli et al., 2016), a pattern that is likely to recur in future warm years (Mueter et al., 2011; Oke et al., 2022).

Beyond influencing pelagic consumers, increases in open-water blooms may also redistribute basal resources away from the benthos. Ice-associated algae commonly comprise large aggregates (Fernández-Méndez et al., 2014; Stabeno et al., 2020), which sink faster than dispersed pelagic algae (Riebesell et al., 1991; Tedesco et al., 2012). Thus, shifts from ice-associated to open-water blooms likely will reduce the magnitude, quality and timing of slower sinking basal resources reaching the seafloor. A reduction in basal resources reaching the sea floor could cause overall decreases to benthic fauna (Grebmeier et al., 2018) that rely heavily on ice algae-derived food sources (Koch et al., 2020), as well as influence lipid accumulation in benthic crabs (Copeman et al., 2021). Whether such changes are linked to recent dramatic declines of commercially important snow crab which were in critical low numbers following the recent warm years 2018-2019 (Fedewa et al., 2020) needs further investigation. If, as predicted, reduced sea ice cover increasingly occurs as the climate continues to warm, the northern Bering Sea may shift from a benthic towards an increasingly pelagically dominated system, more resembling that of the southeastern Bering Sea ecosystem.

Declaration of Competing Interest

The authors declare no known competing financial interests or personal relationships that could have appeared to influence the work reported in this manuscript.

Acknowledgments

We thank Alison Deary and David Kimmel, and two anonymous reviewers for invaluable comments that greatly improved the manuscript. We thank Heather Nibert for making Figure 6. This project is part of the Innovative Technology for Arctic Exploration (ITAE) program funded by NOAA's Pacific Marine Environmental Laboratory (NOAA/PMEL). Funding was also provided by the National Oceanographic Partnership Program (NOPP), and is partially funded by the Cooperative Institute for Climate, Ocean, & Ecosystem Studies (CIOCES) under NOAA Cooperative Agreement NA20OAR4320271. We are grateful for the NCEP Reanalysis data provided by the NOAA/OAR/ESRL PSL, Boulder, Colorado, USA, from their web site at https://psl.noaa.gov. The findings and conclusions in this paper are those of the authors and do not necessarily represent the views of the National Marine Fisheries Service, NOAA. Reference to trade names does not imply endorsement by the National Marine Fisheries Service, NOAA. This is EcoFOCI contribution number EcoFOCI-1031, PMEL contribution number 5448 and CICOES contribution number 2022-1241.

References

Alkama, R., Koffi, E.N., Vavrus, S.J., Diehl, T., Francis, J.A., Stroeve, J., Forzieri, G., Vihma, T., Cescatti, A., 2020. Wind amplifies the polar sea ice retreat. *Environ Res Lett*, 15, 124022.

Arrigo, K.R., Perovich, D.K., Pickart, R.S., Brown, Z.W., van Dijken, G.L., Lowry, K.E., Mills, M.M., Palmer, M.A., Balch, W.M., Bates, N.R., 2014. Phytoplankton blooms beneath the sea ice in the Chukchi Sea. *Deep Sea Research Part II: Topical Studies in Oceanography*, 105, 1-16.

Baier, C.T., Napp, J.M., 2003. Climate-induced variability in *Calanus marshallae* populations. *Journal of Plankton Research*, 25, 771-782.

Baker, M.R., Kivva, K.K., Pisareva, M.N., Watson, J.T., Selivanova, J., 2020. Shifts in the physical environment in the Pacific Arctic and implications for ecological timing and conditions. *Deep Sea Research Part II: Topical Studies in Oceanography*, 177, 104802.

Ballinger, T.J., Overland, J.E., 2022. The Alaskan Arctic regime shift since 2017: A harbinger of years to come? *Polar Science*, 32, 100841.

493 Basyuk, E., Zuenko, Y., 2020. Extreme oceanographic conditions in the northwestern Bering Sea
494 in 2017–2018. *Deep Sea Research Part II: Topical Studies in Oceanography*, 181, 104909.
495 Breiman, L., Friedman, J.H., Olshen, R.A., Stone, C.J., 2017. *Classification and regression*
496 *trees*: Routledge.
497 Brown, Z.W., Arrigo, K.R., 2013. Sea ice impacts on spring bloom dynamics and net primary
498 production in the Eastern Bering Sea. *Journal of Geophysical Research: Oceans*, 118, 43-62.
499 Brown, Z.W., Van Dijken, G.L., Arrigo, K.R., 2011. A reassessment of primary production and
500 environmental change in the Bering Sea. *Journal of Geophysical Research: Oceans*, 116.
501 Burnham, K., Anderson, D., 2002. Model selection and multimodel inference: a practical
502 information-theoretic approach. The University of Chicago Press New York.
503 Cheng, W., Hermann, A.J., Hollowed, A.B., Holsman, K.K., Kearney, K.A., Pilcher, D.J., Stock,
504 C.A., Aydin, K.Y., 2021. Eastern Bering Sea shelf environmental and lower trophic level
505 responses to climate forcing: Results of dynamical downscaling from CMIP6. *Deep Sea*
506 *Research Part II: Topical Studies in Oceanography*, 193, 104975.
507 Chiswell, S.M., Calil, P.H., Boyd, P.W., 2015. Spring blooms and annual cycles of
508 phytoplankton: a unified perspective. *Journal of Plankton Research*, 37, 500-508.
509 Chmura, H.E., Kharouba, H.M., Ashander, J., Ehlman, S.M., Rivest, E.B., Yang, L.H., 2019.
510 The mechanisms of phenology: the patterns and processes of phenological shifts. *Ecological*
511 *Monographs*, 89, e01337.
512 Coachman, L., 1986. Circulation, water masses, and fluxes on the southeastern Bering Sea shelf.
513 *Continental Shelf Research*, 5, 23-108.
514 Cole, H., Henson, S., Martin, A., Yool, A., 2012. Mind the gap: The impact of missing data on
515 the calculation of phytoplankton phenology metrics. *Journal of Geophysical Research: Oceans*,
516 117.
517 Copeman, L.A., Ryer, C.H., Eisner, L.B., Nielsen, J.M., Spencer, M.L., Iseri, P.J., Ottmar, M.L.,
518 2021. Decreased lipid storage in juvenile Bering Sea crabs (*Chionoecetes* spp.) in a warm (2014)
519 compared to a cold (2012) year on the southeastern Bering Sea. *Polar Biology*, 1-19.
520 Coyle, K., Gibson, G., 2017. Calanus on the Bering Sea shelf: probable cause for population
521 declines during warm years. *Journal of Plankton Research*, 39, 257-270.
522 Cushing, D., 1990. Plankton production and year-class strength in fish populations: an update of
523 the match/mismatch hypothesis. *Advances in Marine Biology*, Vol. 26 (pp. 249-293): Elsevier.
524 Dai, Y., Yang, S., Zhao, D., Hu, C., Xu, W., Anderson, D.M., Li, Y., Song, X.-P., Boyce, D.G.,
525 Gibson, L., 2023. Coastal phytoplankton blooms expand and intensify in the 21st century.
526 *Nature*, 615, 280-284.
527 Duffy-Anderson, J.T., Stabeno, P., Andrews Iii, A.G., Cieciel, K., Deary, A., Farley, E., Fugate,
528 C., Harpold, C., Heintz, R., Kimmel, D., Kuletz, K., Lamb, J., Paquin, M., Porter, S., Rogers, L.,
529 Spear, A., Yasumiishi, E., 2019. Responses of the Northern Bering Sea and Southeastern Bering
530 Sea Pelagic Ecosystems Following Record-Breaking Low Winter Sea Ice. *Geophysical Research*
531 *Letters*, 46, 9833-9842.
532 Eisner, L.B., Gann, J.C., Ladd, C., Cieciel, K.D., Mordy, C.W., 2016. Late summer/early fall
533 phytoplankton biomass (chlorophyll a) in the eastern Bering Sea: Spatial and temporal variations
534 and factors affecting chlorophyll a concentrations. *Deep Sea Research Part II: Topical Studies in*
535 *Oceanography*, 134, 100-114.
536 Eisner, L.B., Yasumiishi, E.M., Andrews III, A.G., O'Leary, C.A., 2020. Large copepods as
537 leading indicators of walleye pollock recruitment in the southeastern Bering Sea: sample-Based
538 and spatio-temporal model (VAST) results. *Fisheries Research*, 232, 105720.

539 Fedewa, E.J., Jackson, T.M., Richar, J.I., Gardner, J.L., Litzow, M.A., 2020. Recent shifts in
540 northern Bering Sea snow crab (Chionoecetes opilio) size structure and the potential role of
541 climate-mediated range contraction. *Deep Sea Research Part II: Topical Studies in*
542 *Oceanography*, 181, 104878.
543 Fernández-Méndez, M., Wenzhöfer, F., Peeken, I., Sørensen, H.L., Glud, R.N., Boetius, A.,
544 2014. Composition, buoyancy regulation and fate of ice algal aggregates in the Central Arctic
545 Ocean. *PLoS One*, 9, e107452.
546 Ferreira, A.S.A., Stige, L.C., Neuheimer, A.B., Bogstad, B., Yaragina, N., Prokopchuk, I.,
547 Durant, J.M., 2020. Match-mismatch dynamics in the Norwegian-Barents Sea system. *Marine*
548 *Ecology Progress Series*, 650, 81-94.
549 Friedland, K.D., McManus, M.C., Morse, R.E., Link, J.S., 2019. Event scale and persistent
550 drivers of fish and macroinvertebrate distributions on the Northeast US Shelf. *ICES Journal of*
551 *Marine Science*, 76, 1316-1334.
552 Grebmeier, J.M., Frey, K.E., Cooper, L.W., Kędra, M., 2018. Trends in benthic macrofaunal
553 populations, seasonal sea ice persistence, and bottom water temperatures in the Bering Strait
554 region. *Oceanography*, 31, 136-151.
555 Hunt, G.L.J., Coyle, K.O., Eisner, L.B., Farley, E.V., Heintz, R.A., Mueter, F., Napp, J.M.,
556 Overland, J.E., Ressler, P.H., Salo, S., 2011. Climate impacts on eastern Bering Sea foodwebs: a
557 synthesis of new data and an assessment of the Oscillating Control Hypothesis. *ICES Journal of*
558 *Marine Science*, 68, 1230-1243.
559 Hunt, G.L.J., Ressler, P.H., Gibson, G.A., De Robertis, A., Aydin, K., Sigler, M.F., Ortiz, I.,
560 Lessard, E.J., Williams, B.C., Pinchuk, A., 2016. Euphausiids in the eastern Bering Sea: A
561 synthesis of recent studies of euphausiid production, consumption and population control. *Deep*
562 *Sea Research Part II: Topical Studies in Oceanography*, 134, 204-222.
563 Ianelli, J.N., Honkalehto, T., Barbeaux, S.J., Fissel, B.E., Kotwicki, S., 2016. Assessment of the
564 walleye pollock stock in the eastern Bering Sea. *In* Stock assessment and fishery evalauation
565 report of the eastern Bering Sea, North Pacific Fishery Management Council, 1007 West 3rd
566 Ave., Suite 400

567 L92 Building, 4th floor, Anchorage, Alaska 99501.
568 Ji, R., Edwards, M., Mackas, D.L., Runge, J.A., Thomas, A.C., 2010. Marine plankton
569 phenology and life history in a changing climate: current research and future directions. *Journal*
570 *of plankton research*, 32, 1355-1368.
571 Ji, R., Jin, M., Varpe, Ø., 2013. Sea ice phenology and timing of primary production pulses in
572 the Arctic Ocean. *Global Change Biology*, 19, 734-741.
573 Kahru, M., Brotas, V., Manzano-Sarabia, M., Mitchell, B.G., 2011. Are phytoplankton blooms
574 occurring earlier in the Arctic? *Global Change Biology*, 17, 1733-1739.
575 Kahru, M., Lee, Z., Mitchell, B.G., Nevison, C.D., 2016. Effects of sea ice cover on satellite-
576 detected primary production in the Arctic Ocean. *Biology letters*, 12, 20160223.
577 Kalnay, E., Kanamitsu, M., Kistler, R., Collins, W., Deaven, D., Gandin, L., Iredell, M., Saha,
578 S., White, G., Woollen, J., 1996. The NCEP/NCAR 40-year reanalysis project. *Bulletin of the*
579 *American Meteorological Society*, 77, 437-472.
580 Kharouba, H.M., Ehrlén, J., Gelman, A., Bolmgren, K., Allen, J.M., Travers, S.E., Wolkovich,
581 E.M., 2018. Global shifts in the phenological synchrony of species interactions over recent
582 decades. *Proceedings of the National Academy of Sciences*, 115, 5211.

583 Kimmel, D.G., Eisner, L.B., Wilson, M.T., Duffy-Anderson, J.T., 2018. Copepod dynamics
584 across warm and cold periods in the eastern Bering Sea: Implications for walleye pollock (*Gadus*
585 *chalcogrammus*) and the Oscillating Control Hypothesis. *Fisheries Oceanography*, 27, 143-158.
586 Kivva, K., Kubryakov, A., 2021. Seasonal and Interannual Variability of Chlorophyll-a
587 Concentration in the Bering Sea Found from Satellite Data. *Izvestiya, Atmospheric and Oceanic*
588 *Physics*, 57, 1643-1657.
589 Kivva, K., Selivanova, Y.V., Pisareva, M., Sumkina, A., 2020. Role of physical processes in
590 formation of spring phytoplankton bloom in the Bering Sea. *Habitat of aquatic biological*
591 *resources*.
592 Koch, C.W., Cooper, L.W., Grebmeier, J.M., Frey, K., Brown, T.A., 2020. Ice algae resource
593 utilization by benthic macro-and megafaunal communities on the Pacific Arctic shelf determined
594 through lipid biomarker analysis. *Marine Ecology Progress Series*, 651, 23-43.
595 Ladd, C., Bond, N.A., 2002. Evaluation of the NCEP/NCAR reanalysis in the NE Pacific and the
596 Bering Sea. *Journal of Geophysical Research: Oceans*, 107, 22-21-22-29.
597 Ladd, C., Stabeno, P.J., 2012. Stratification on the Eastern Bering Sea shelf revisited. *Deep Sea*
598 *Research Part II: Topical Studies in Oceanography*, 65-70, 72-83.
599 Maritorena, S., d'Andon, O.H.F., Mangin, A., Siegel, D.A., 2010. Merged satellite ocean color
600 data products using a bio-optical model: Characteristics, benefits and issues. *Remote Sensing of*
601 *Environment*, 114, 1791-1804.
602 Mioduszewski, J., Vavrus, S., Wang, M., 2018. Diminishing Arctic sea ice promotes stronger
603 surface winds. *Journal of Climate*, 31, 8101-8119.
604 Mueter, F.J., Bond, N.A., Ianelli, J.N., Hollowed, A.B., 2011. Expected declines in recruitment
605 of walleye pollock (Theragra chalcogramma) in the eastern Bering Sea under future climate
606 change. *ICES Journal of Marine Science*, 68, 1284-1296.
607 Mueter, F.J., Planque, B., Hunt Jr, G.L., Alabia, I.D., Hirawake, T., Eisner, L., Dalpadado, P.,
608 Chierici, M., Drinkwater, K.F., Harada, N., 2021. Possible future scenarios in the gateways to the
609 Arctic for Subarctic and Arctic marine systems: II. prey resources, food webs, fish, and fisheries.
610 *ICES Journal of Marine Science*, 78, 3017-3045.
611 Niebauer, H., Alexander, V., Henrichs, S.M., 1995. A time-series study of the spring bloom at
612 the Bering Sea ice edge I. Physical processes, chlorophyll and nutrient chemistry. *Continental*
613 *Shelf Research*, 15, 1859-1877.
614 Oke, K.B., Mueter, F., Litzow, M.A., 2022. Warming leads to opposite patterns in weight-at-age
615 for young versus old age classes of Bering Sea walleye pollock. *Canadian Journal of Fisheries*
616 *and Aquatic Sciences*, 79, 1655-1666.
617 Perrette, M., Yool, A., Quartly, G., Popova, E.E., 2011. Near-ubiquity of ice-edge blooms in the
618 Arctic. *Biogeosciences*, 8, 515-524.
619 Pierson, J.J., Batchelder, H., Saumweber, W., Leising, A., Runge, J., 2013. The impact of
620 increasing temperatures on dormancy duration in Calanus finmarchicus. *Journal of plankton*
621 *research*, 35, 504-512.
622 R Core Team, 2018. R: A Language and Environment for Statistical Computing, R Foundation
623 for Statistical Computing, Austria, 2015. ISBN 3-900051-07-0: URL http://www. R-project. org.
624 Riebesell, U., Schloss, I., Smetacek, V., 1991. Aggregation of algae released from melting sea
625 ice: implications for seeding and sedimentation. *Polar Biology*, 11, 239-248.
626 Saitoh, S.-i., Iida, T., Sasaoka, K., 2002. A description of temporal and spatial variability in the
627 Bering Sea spring phytoplankton blooms (1997–1999) using satelite multi-sensor remote
628 sensing. *Prog Oceanogr*, 55, 131-146.

Sambrotto, R., Niebauer, H., Goering, J., Iverson, R., 1986. Relationships among vertical mixing, nitrate uptake, and phytoplankton growth during the spring bloom in the southeast Bering Sea middle shelf. *Continental Shelf Research*, 5, 161-198.
Siddon, E.C., Kristiansen, T., Mueter, F.J., Holsman, K.K., Heintz, R.A., Farley, E.V., 2013. Spatial match-mismatch between juvenile fish and prey provides a mechanism for recruitment variability across contrasting climate conditions in the eastern Bering Sea. *PLoS One*, 8, e84526.
Sigler, M.F., Napp, J.M., Stabeno, P.J., Heintz, R.A., Lomas, M.W., Hunt Jr, G.L., 2016. Variation in annual production of copepods, euphausiids, and juvenile walleye pollock in the southeastern Bering Sea. *Deep Sea Research Part II: Topical Studies in Oceanography*, 134, 223-234.
Sigler, M.F., Stabeno, P.J., Eisner, L.B., Napp, J.M., Mueter, F.J., 2014. Spring and fall phytoplankton blooms in a productive subarctic ecosystem, the eastern Bering Sea, during 1995–2011. *Deep Sea Research Part II: Topical Studies in Oceanography*, 109, 71-83.
Skirving, W., Marsh, B., De La Cour, J., Liu, G., Harris, A., Maturi, E., Geiger, E., Eakin, C.M., 2020. Coraltemp and the coral reef watch coral bleaching heat stress product suite version 3.1. *Remote Sensing*, 12, 3856.
Song, H., Ji, R., Jin, M., Li, Y., Feng, Z., Varpe, Ø., Davis, C.S., 2021. Strong and regionally distinct links between ice-retreat timing and phytoplankton production in the Arctic Ocean. *Limnology and Oceanography*.
Springer, A.M., McRoy, C.P., Flint, M.V., 1996. The Bering Sea Green Belt: shelf-edge processes and ecosystem production. *Fisheries Oceanography*, 5, 205-223.
Stabeno, P.J., Bell, S.W., 2019. Extreme Conditions in the Bering Sea (2017–2018): Record-Breaking Low Sea-Ice Extent. *Geophysical Research Letters*, 46, 8952-8959.
Stabeno, P.J., Farley Jr, E.V., Kachel, N.B., Moore, S., Mordy, C.W., Napp, J.M., Overland, J.E., Pinchuk, A.I., Sigler, M.F., 2012a. A comparison of the physics of the northern and southern shelves of the eastern Bering Sea and some implications for the ecosystem. *Deep Sea Research Part II: Topical Studies in Oceanography*, 65, 14-30.
Stabeno, P.J., Hunt, G.L.J., 2002. Overview of the inner front and southeast Bering Sea carrying capacity programs. *Deep Sea Research Part II: Topical Studies in Oceanography*, 49, 6157-6168.
Stabeno, P.J., Kachel, N.B., Moore, S.E., Napp, J.M., Sigler, M., Yamaguchi, A., Zerbini, A.N., 2012b. Comparison of warm and cold years on the southeastern Bering Sea shelf and some implications for the ecosystem. *Deep Sea Research Part II: Topical Studies in Oceanography*, 65, 31-45.
Stabeno, P.J., Mordy, C.W., Sigler, M.F., 2020. Seasonal patterns of near-bottom chlorophyll fluorescence in the eastern Chukchi Sea: 2010–2019. *Deep Sea Research Part II: Topical Studies in Oceanography*, 177, 104842.
Staudinger, M.D., Mills, K.E., Stamieszkin, K., Record, N.R., Hudak, C.A., Allyn, A., Diamond, A., Friedland, K.D., Golet, W., Henderson, M.E., Hernandez, C.M., Huntington, T.G., Ji, R., Johnson, C.L., Johnson, D.S., Jordaan, A., Kocik, J., Li, Y., Liebman, M., Nichols, O.C., Pendleton, D., Richards, R.A., Robben, T., Thomas, A.C., Walsh, H.J., Yakola, K., 2019. It's about time: A synthesis of changing phenology in the Gulf of Maine ecosystem. *Fisheries Oceanography*, 0, 532-566.
Syvertsen, E.E., 1991. Ice algae in the Barents Sea: types of assemblages, origin, fate and role in the ice-edge phytoplankton bloom. *Polar Research*, 10, 277-288.

Tedesco, L., Vichi, M., Thomas, D.N., 2012. Process studies on the ecological coupling between sea ice algae and phytoplankton. *Ecological Modelling*, 226, 120-138.
Therneau, T., Atkinson, B., Ripley, B., Ripley, M.B., 2015. Package 'rpart'. *Available online: cran. ma. ic. ac. uk/web/packages/rpart/rpart. pdf*.
Waga, H., Eicken, H., Hirawake, T., Fukamachi, Y., 2021. Variability in spring phytoplankton blooms associated with ice retreat timing in the Pacific Arctic from 2003–2019. *Plos One*, 16, e0261418.
Walsh, J.E., Ballinger, T.J., Euskirchen, E.S., Hanna, E., Mård, J., Overland, J.E., Tangen, H., Vihma, T., 2020. Extreme weather and climate events in northern areas: A review. *Earth-Science Reviews*, 209, 103324.
Wickham, H., Chang, W., 2009. ggplot2: An implementation of the Grammar of Graphics. R package version 0.8. 3.
Wickham, H., François, R., Henry, L., Müller, K., 2019. dplyr: a grammar of data manipulation. R package version 0.8. 0.1. *Retrieved January*, 13, 2020.
Wood, S., Wood, M.S., 2015. Package 'mgcv'. *R package version*, 1-7.

TABLES AND FIGURES

Figure 1

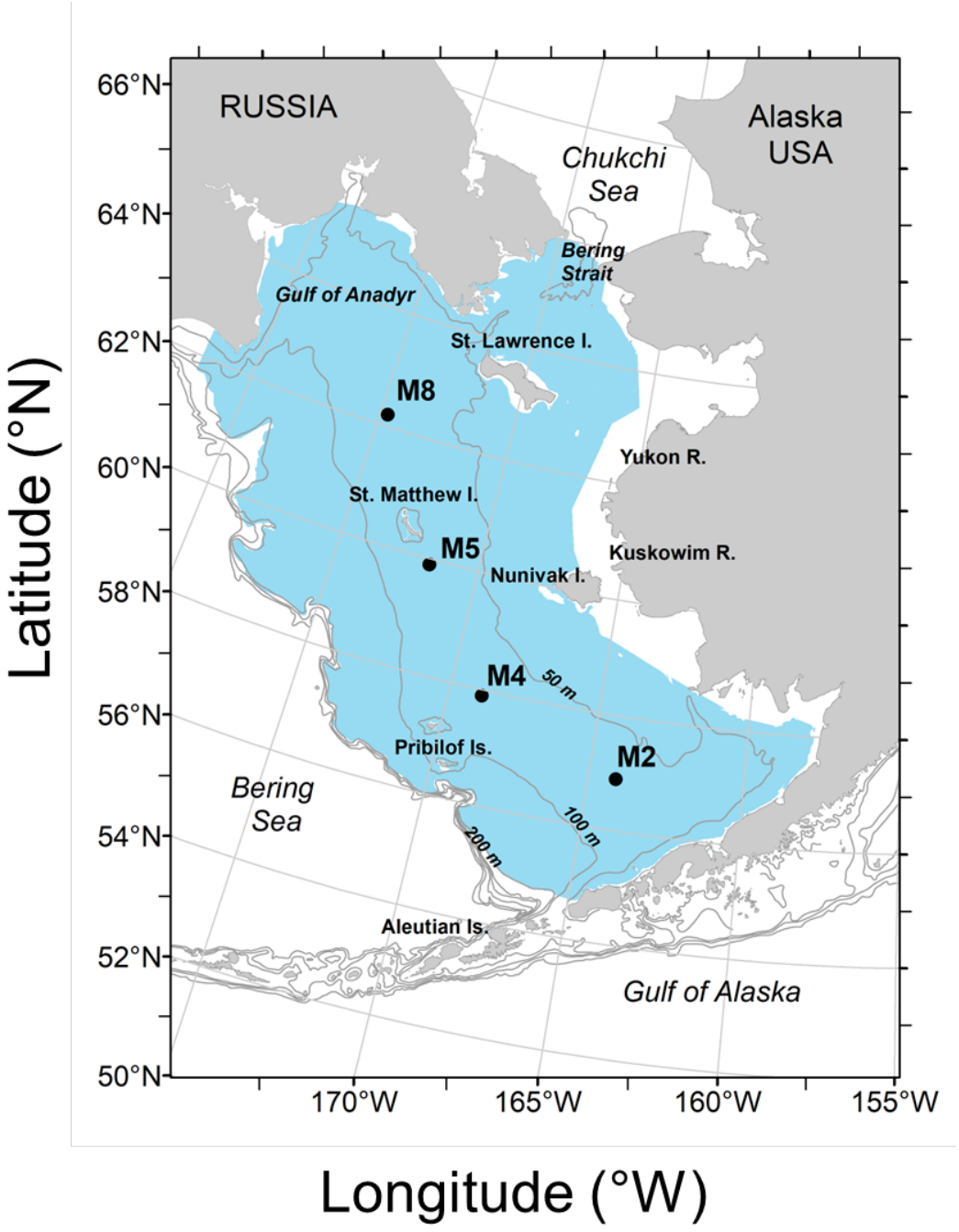

Fig. 1: Map of the Bering Sea, showing the mooring (M2, M4, M5 and M8) locations and the study area (blue, bottom depth 20-180 m).

Figure 2

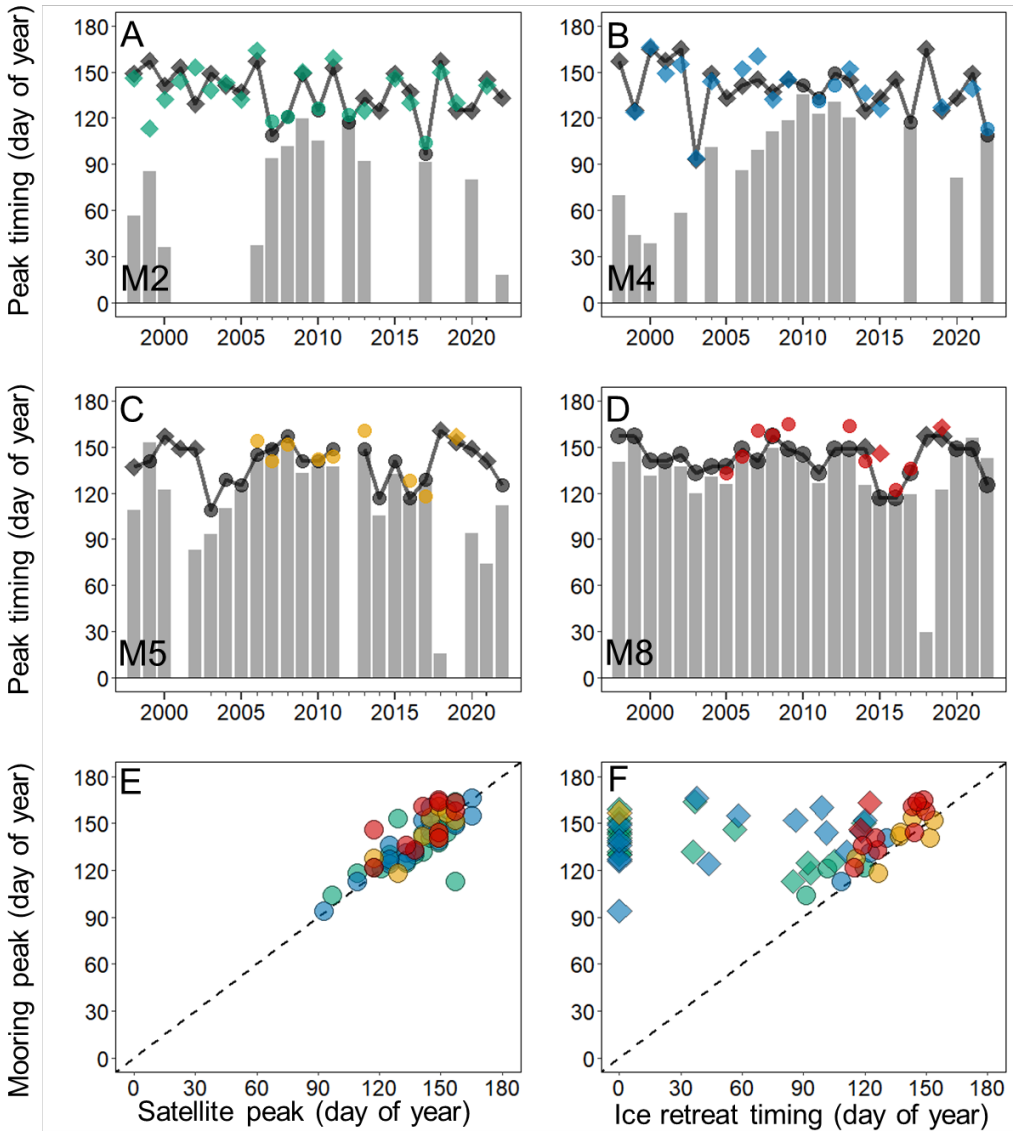

Fig. 2: Spring peak bloom timing estimates (day of year) from Chl-*a* MODIS satellite data (black) and Chl-*a* from the moorings **A**) M2 (green), **B**) M4 (blue), **C**) M5 (orange) and **D**) M8 (red) from 1998 to 2022. The bloom generally occurs in two forms, an open-water bloom (diamonds) in association with the onset of thermal stratification, or an ice-associated bloom (circles) regulated by the timing of ice retreat. Grey shaded bars denotes timing of ice retreat (estimated as the day of year when ice cover decreased to below 15 %). **E)** Comparison of Chl-*a* peak bloom timing estimates from MODIS satellite data and moorings ($r = 0.75$, $p < 0.01$) and **F**) ice retreat timing and mooring bloom peak timing estimates. An ice retreat timing of zero indicates no sea ice formed around the mooring location in that year (though ice could have formed briefly in the fall the prior year). The 1:1 line is shown in black, and moorings are color coded in **E** and **F** as in **A-D**.

Figure 3

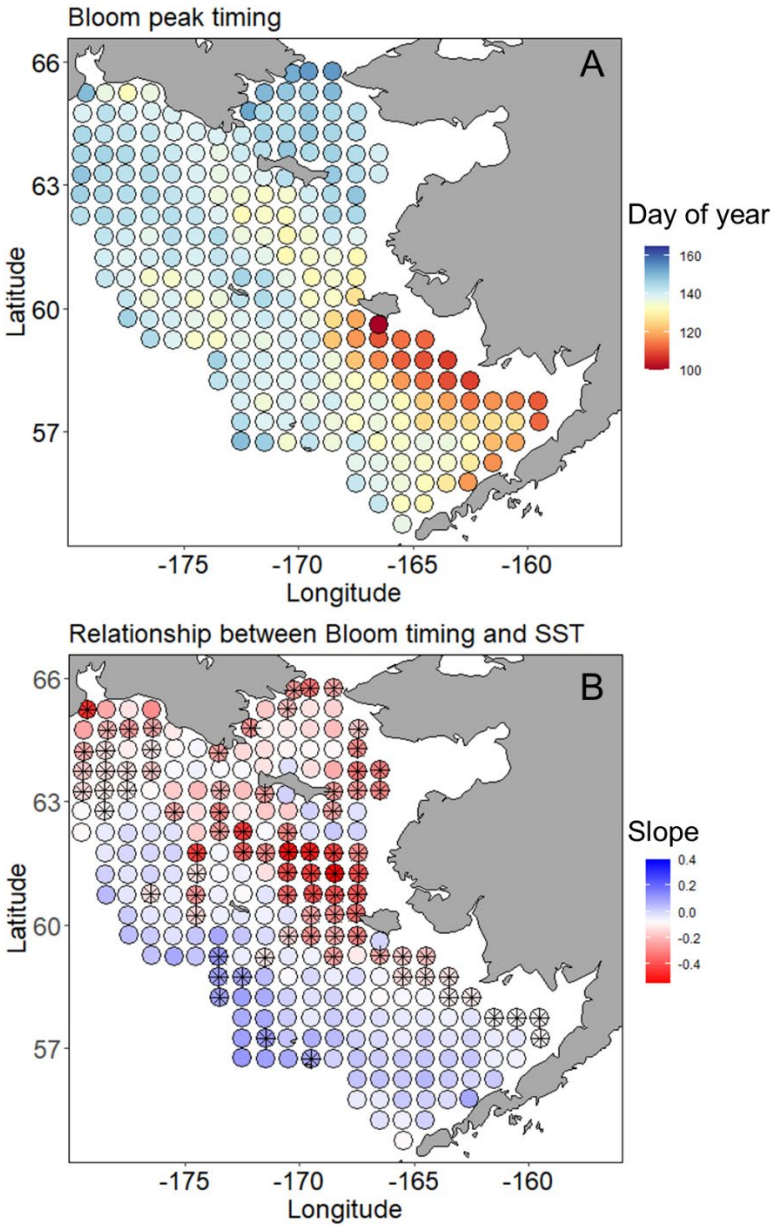

Fig. 3: Spatial overview of **A)** average bloom timing for all years (1998-2022) and **B)** correlation with the cumulative spring SST anomalies estimates using robust linear regression analyses. For **B)** colors show the value of the slope from a regression of bloom timing as a function of cumulative SST anomaly and the presence of a "star" inside a circle denotes when the relationship is significant ($p < 0.05$). Annual bloom timing (1998-2022, Fig. S2) are available in the Supplementary information.

Figure 4

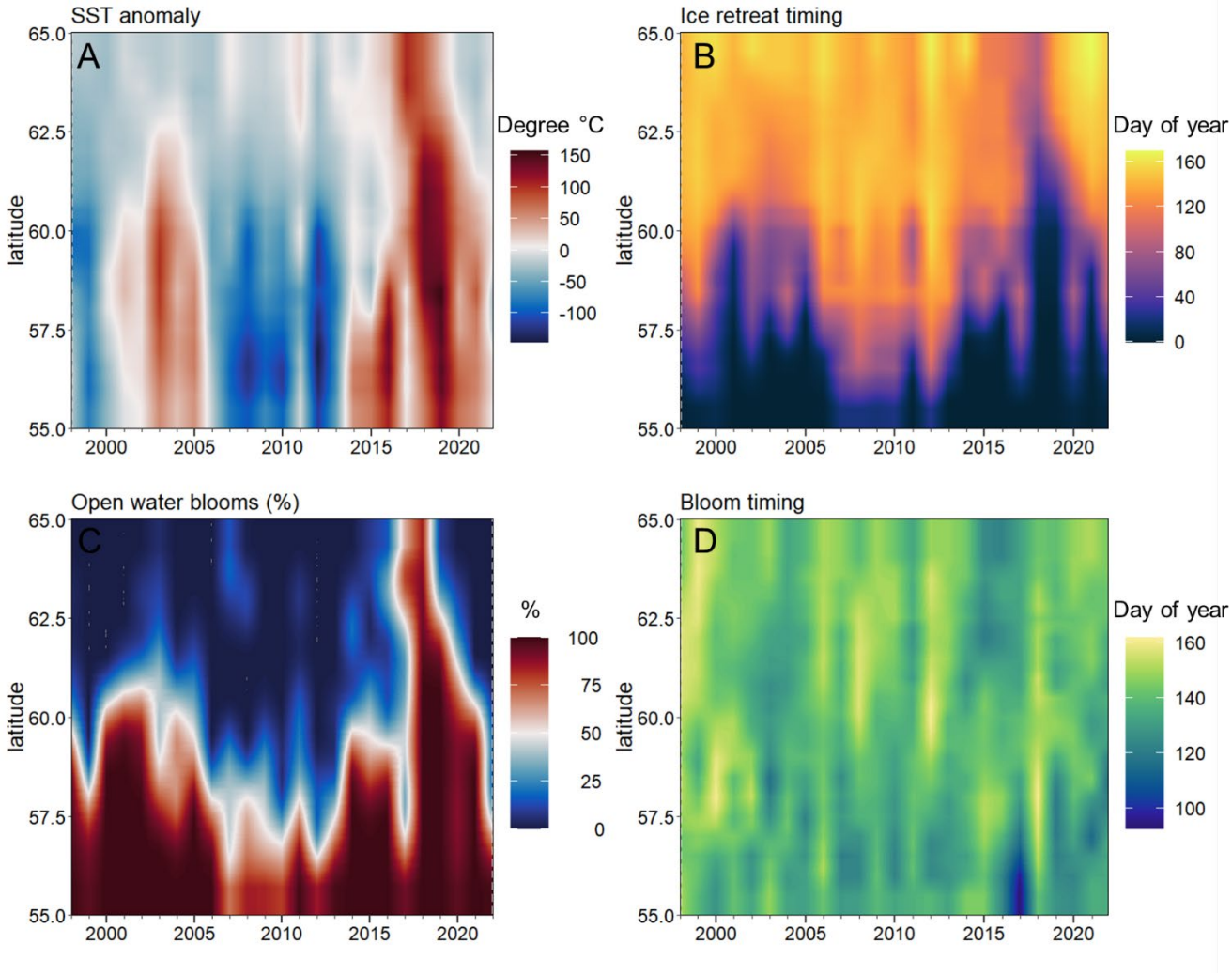

Fig. 4: Hovmuller diagrams (year-latitude) for averaged across the middle and outer shelf regions (bottom depth: 50 - 180 m) showing temporal and spatial changes for, **A)** cumulative Sea surface temperature anomalies (°C) , **B)** timing of ice retreat (day of year), **C)** percentage of open-water blooms (%, blooms occurring at least 21 days after the day of ice retreat timing) and **D)** phytoplankton spring bloom peak timing (day of year).

Figure 5

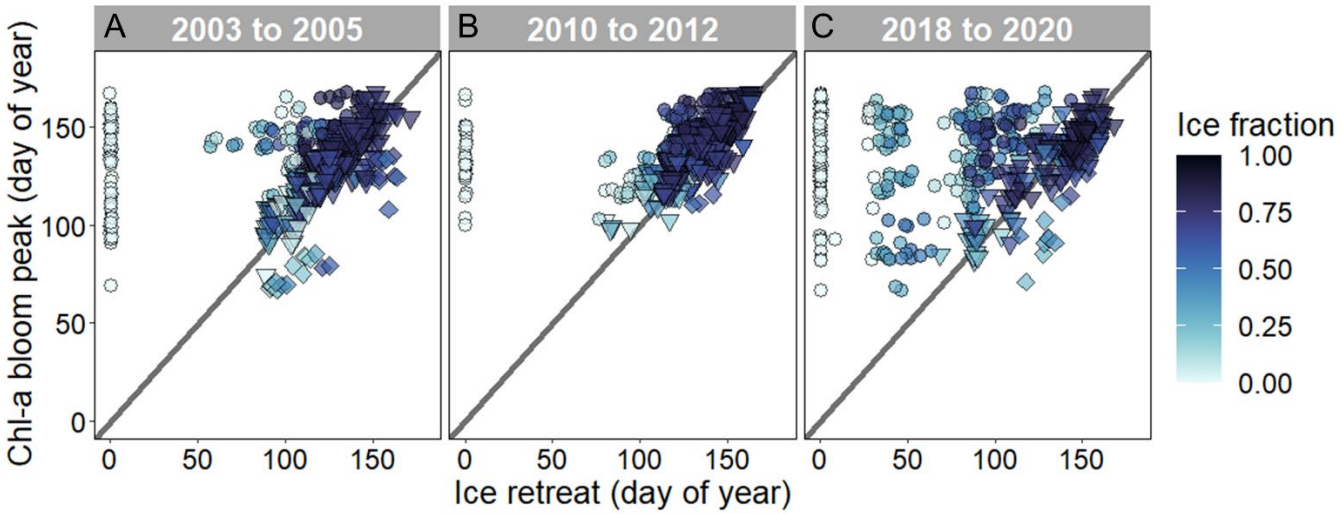

Fig. 5: Correlation between satellite estimates of the timing of ice retreat and peak timing of open-water (circle), ice-associated (triangle), and earlier than ice retreat (diamonds) blooms estimated for years during the early warm period (2003 - 2005), the cold period (2010 - 2012) and the recent warm period (2018 - 2020) in the eastern Bering Sea. Color code shows average ice fraction (0-1) from 1 February to time of ice retreat for each area. 1:1 line shown in grey. Ice retreat was estimated as the day when ice fractional cover decreased to below 15 %.

Figure 6

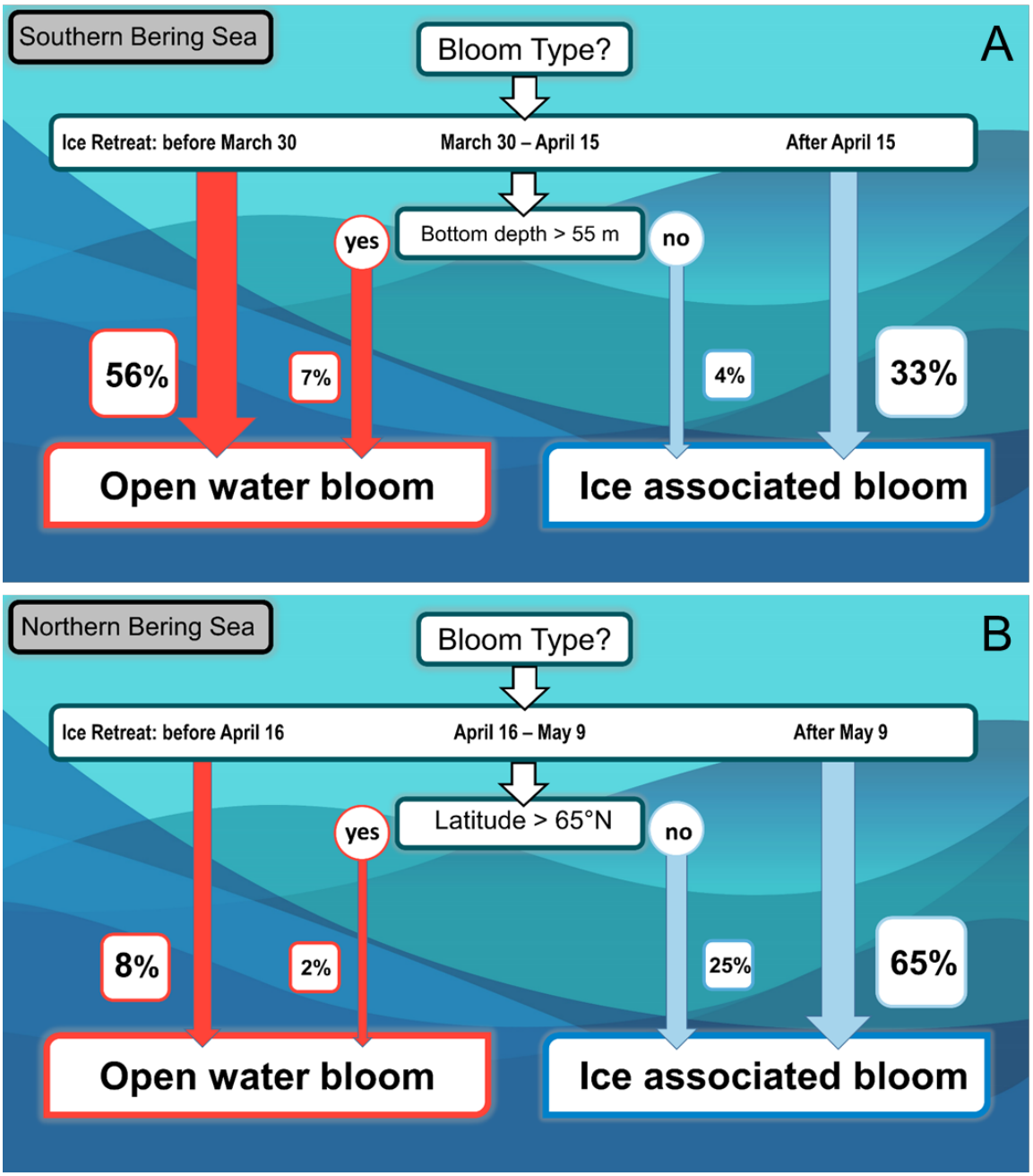

Fig. 6: Classification Decision Tree analysis showing which variables influence the formation of open-water versus ice-associated bloom formation on the **A**) southern and **B**) northern Bering Sea shelf. Percentages denote the proportion of bloom types following each pathway.

Figure 7

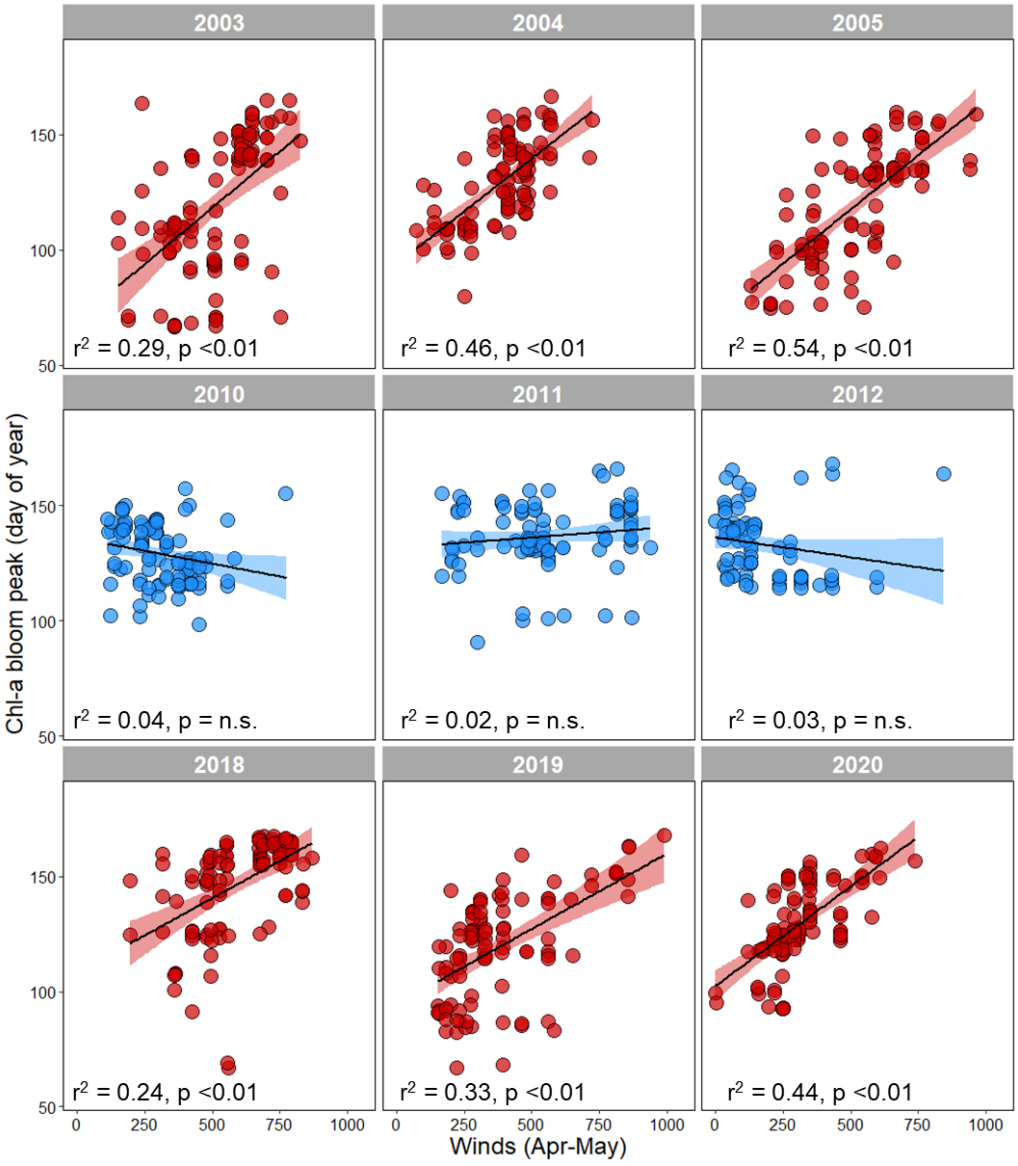

Fig 7: Relationship between cumulative wind speed metric (Apr-May) and Chl-*a* bloom peak timing (day of year) during the early warm period (2003 – 2005, red, top panel), the cold period (2010 – 2012, blue, middle panel) and the recent warm period (2018 – 2020, red, bottom panel) for the southern (< 60° N) Bering Sea. Plots for the same years for the northern Bering Sea are available in the Supplementary information (Fig. S4). n.s. = not significance.

Figure 8

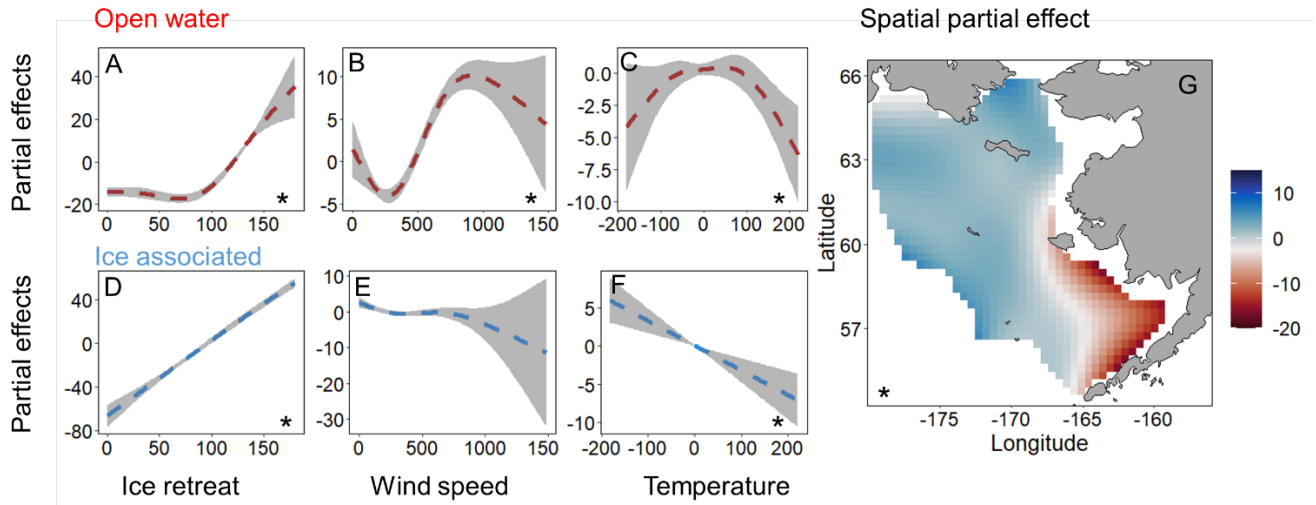

Fig. 8: Partial effect plots, which are used to assess the isolated effects of a particular predictor or interaction, of the most parsimonious GAM (model B). Showing bloom timing response for open-water blooms (top row) and ice-associated blooms (bottom row) to **A, D**) ice retreat timing (day of year), **B, E**) wind speed metric (m/s), **C, F)** cumulative SST anomaly (°C) and **G**) spatial variation (longitude, latitude). Bloom type was noted as open water when ice retreat was > 21 days before bloom peak timing, while ice associated bloom denote blooms occurring ≤ 21 days after ice retreat timing. Note different y-scales for each graph. Wind speed metric is a cumulative score of wind events 10-15 m/s with a duration of at least 24 hours during April and May. * denote significant explanatory variables. Note year random effect not shown

Figure 9

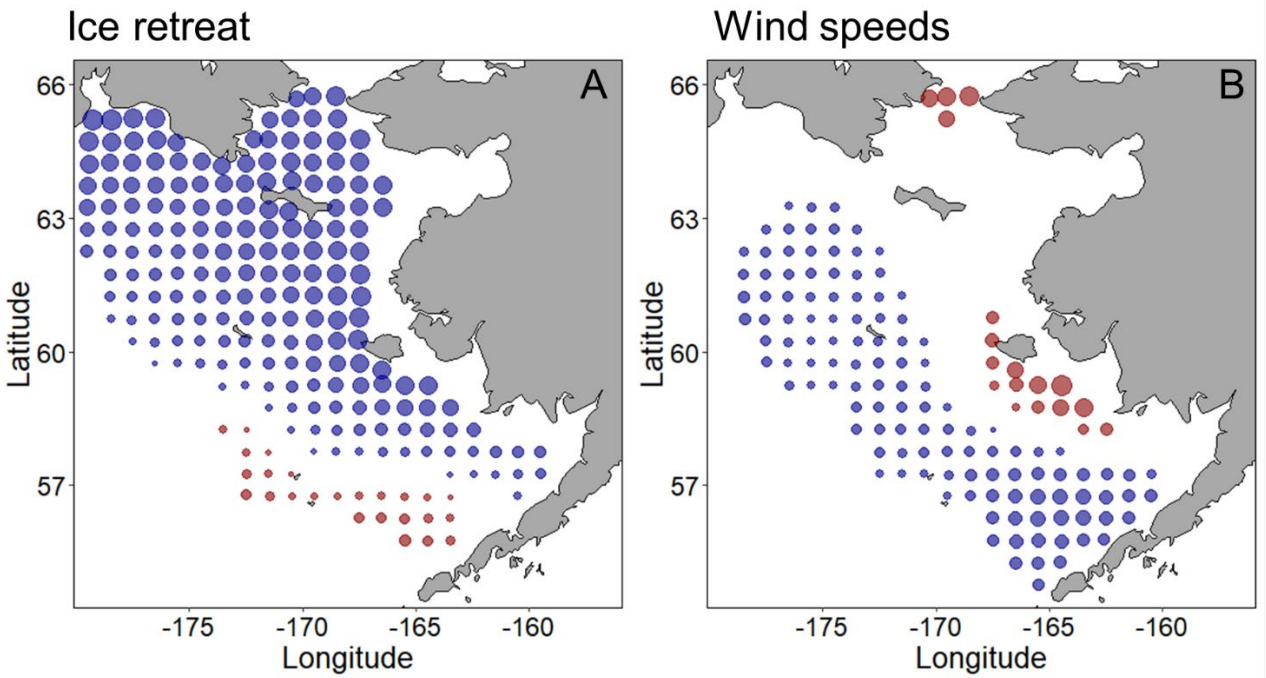

Fig. 9: Spatial GAM prediction for **A**) ice retreat as a spatial slope effect (model C) and **B**) wind speed modeled as a spatial slope effect (model D), which was done only for open water bloom types. Blue circles indicate statistically significant positive slopes ($p < 0.05$) between bloom timing and ice retreat or winds (e.g., higher wind speed metric associates with later bloom timing), while red circles denote statistically negative slopes between bloom timing and predictor variables. The size of the circle shows the steepness of the slope.